# Perihematomal Cerebral Tissue Iron Quantification on MRI Following Intracerebral Hemorrhage in Two Human Subjects: Proof of Principle

Neeraj Chaudhary, Aditya S. Pandey, Kevin Merchak, Joseph J. Gemmete, Tom Chenevert, and Guohua Xi

## Introduction

Each year, approximately 800,000 people suffer a stroke in the United States. The causes of stroke are, in general, either hemorrhagic or nonhemorrhagic. Intracranial hemorrhage (ICH) is a common and often fatal stroke subtype [1, 2]. More than 30,000 patients die from spontaneous ICH annually. Iron has a major role in ICH-induced brain injury [1, 3, 4]. There is a progressive accumulation of iron in the cerebral tissue surrounding a hematoma from hemoglobin degradation within the hematoma as it resolves. The high level of non-heme iron remains in the brain for at least 1 month [5]. By enhanced Perls' reaction, iron-positive cells are found in the perihematomal zone as early as the first day [5]. Our studies also have shown that free iron levels in cerebrospinal fluid (CSF) increase almost 14-fold after ICH on the third day and remain high for at least 28 days after experimental ICH [7]. Increases of brain iron levels cause brain edema, oxidative stress, brain atrophy, and neurological deficits following ICH [1, 6, 8].

If the patient survives the ictus, the resulting hematoma within brain parenchyma triggers a series of events leading to secondary insults and severe neurological deficits [9]. There is currently no proven therapy for ICH other than supportive care [10, 11]. Although the hematoma in humans gradually resolves, neurological deficits in ICH patients are usually permanent and disabling. Iron has a major role in brain damage following ICH [1, 11]. Brain injury after ICH appears to involve several phases [1]. These include an early phase involving the clotting cascade activation and thrombin production [10–16] and a later phase involving erythrocyte lysis and iron toxicity [2–4, 17–19]. After erythrocyte lysis within the hematoma, iron concentrations in surrounding brain can reach very high levels. Studies have shown that high levels of serum ferritin, an iron-binding protein, are independently associated with poor outcome and severe brain edema in ICH patients [16, 17].

It is well known that iron has a key role in brain edema formation following ICH [1, 19]. Perihematomal brain edema develops immediately after ICH and peaks several days later [6, 19]. Edema formation following ICH elevates intracranial pressure and may result in herniation [20]. In experimental ICH models, brain edema peaks around the third or fourth day after the hemorrhage then declines slowly [10, 21–23]. In species with significant white matter, perihematomal edema is mainly located within that tissue [22]. In humans, perihematomal edema develops within 3 h of symptom onset and peaks between 10 and 20 days after the ictus [23]. Several studies show that the degree of brain edema around the hematoma correlates with poor outcome in patients [20, 24, 25]. We have shown that desferoxamine, an iron chelate, reduces brain edema and hemorrhagic brain injury in aged rats and pigs [26–28]. Deferoxamine has been examined by a phase I trial in human subjects [29]. The promise it has shown in these trials has led to a further phase II trial, which was approved by the NIH.

Although there is a growing body of evidence for the role of iron in neuronal damage following parenchymal hemorrhage, there is a conspicuous lack of a reliable paradigm for accurate quantification of the tissue iron load. Interest in

N. Chaudhary, MD, MRCS, FRCR (✉)
Neurointerventional Radiology, Departments of Radiology & Neurosurgery, University of Michigan, Ann Arbor, MI, USA
e-mail: neerajc@med.umich.edu

A.S. Pandey, MD • J.J. Gemmete, MD FACR FSIR
Departments of Neurosurgery and Radiology, University of Michigan, Ann Arbor, MI, USA

K. Merchak
Department of Biomed Engineering, University of Michigan, Ann Arbor, MI, USA

T. Chenevert, PhD
Department of Radiology, University of Michigan, Ann Arbor, MI, USA

G. Xi, MD
Department of Neurosurgery, University of Michigan, Ann Arbor, MI, USA

R.L. Applegate et al. (eds.), *Brain Edema XVI: Translate Basic Science into Clinical Practice*, Acta Neurochirurgica Supplement, Vol. 121,
DOI 10.1007/978-3-319-18497-5_32, 

noninvasive quantification of tissue iron has resurged with development of effective iron chelate therapy in prevention of iron toxicity [30]. Existing noninvasive modalities such as magnetic resonance imaging (MRI) have been utilized to develop iron measurement algorithms in the heart [31]. Traumatic brain injury is another condition where MRI-based estimation of iron deposition in the cerebral tissue has been explored [32, 33]. Human physiology is incapable of excreting excess iron. Iron is deposited in various tissues in the body in clinical conditions that require repeated blood transfusions. Paramagnetic effects of tissue-deposited iron, causing signal inhomogeneity on MRI, have been exploited to estimate tissue iron levels in human visceral tissue [30, 31, 34]. Although some advances have been made in quantifying iron in the human liver by MRI, a robust technique has not been developed yet [35, 36]. Bilgic et al. [37] have demonstrated feasibility of detection of iron levels in brain tissue of normal aging population by quantitative susceptibility mapping (QSM). They demonstrated specificity of the field-dependent relaxation rate (FDRI) technique in detection of minute concentrations of iron in the brain tissue with age. Preliminary clinical studies have demonstrated the ability to detect cerebral tissue iron in traumatic brain injury by utilizing T2* magnetic field correlation on MRI [32]. Liu et al. [38], utilizing a porcine model, demonstrated the ability of R2 (1/T2) relaxivity maps in detecting superparamagnetic iron oxide (SPIO) nanoparticles in the brain tissue following disruption of blood brain barrier (BBB) by low-frequency ultrasound. Sammet et al. [39] showed the importance of multiple spin echo sequences on MRI for reliable correlation with iron levels and developed a mathematical model to differentiate between ferritin and hemosiderin on MRI using an agarose-phantom. In a porcine ICH model, utilizing 7 T MRI, Wu et al. [40] demonstrated the application of T2* sequences to correlate with hematoma size and histopathological evidence of tissue iron. A study from Wang et al. [41] showed the reliability of QSM on T2* MRI scan in patients with ICH. They utilized the application of R2* (1/T2*) relaxivity maps to obtain a reliable calculation of hematoma volume.

At the time of this writing, there have been no studies performed to ascertain accurate tissue iron levels at the periphery of the hematoma in patients with ICH. Our hypothesis is that MRI is sensitive enough to pick up field inhomogeneity due to the presence of excess brain tissue iron. A reliable MR-based iron quantification algorithm can be beneficial in management of patients with ICH. It can serve as a surrogate marker of severity of neurotoxicity. Once validated, it can serve to monitor efficacy of the iron-chelating agents like deferoxamine currently being tested in this patient population. Above all, it may possibly enable prediction of ICH in patients if correlation of brain tissue iron levels can be demonstrated with functional outcome in the future.

## Materials and Methods

### MRI Phantom Construction

Institutional Review Board approval was obtained to perform MRI scans on selected patients with ICH. Initially, we constructed a phantom with varying concentrations of iron and then scanned the phantom in a 3 T MRI. The phantom was constructed with a cylindrical container made out of material that would not cause signal aberration on MRI; a plastic cylindrical container was utilized. A liquid iron preparation, ferumoxytol (Feraheme®, AMAG Pharmaceuticals, Waltham, MA, USA), which is used for intravenous ferrous sulfate therapy, was selected as the appropriate liquid preparation. It is a non-stoichiometric magnetite (superparamagnetic iron oxide) coated with polyglucose sorbitol carboxymethylether.

We then prepared serial dilutions of the ferumoxytol in seven different reducing dilutions, commencing with 6 mg/ml and ending with 0.0047 mg/ml. Each subsequent concentration was 50 % less than the prior. The above concentrations were chosen as the iron concentrations in the published literature lie in the middle of the above distribution. Four milliliters of each concentration was placed in a 4-ml glass vial, avoiding any air bubbles. Seven glass vials were then attached to the undersurface of the lid of the plastic container selected for the phantom (Fig 1a), which was then filled with sterile water to replace any air bubbles in the container. The phantom was scanned in a 3 T MRI with the following susceptibility weighted sequences: 3D TR = 40 ms, TE = 6.5, 11, 15.5, 20, 24.5, 29, 33.5, 38 ms, 1.5 mm slice-to-slice, acquired as 3 mm, acquired resolution matrix = 240 × 240, FOV – 240 mm × 240 mm (Fig 1b). T2* signal magnitude measurements were then obtained corresponding to these concentrations (Table 1).

### Human Subjects Scanned

ICH patients, age 18–85 years, with brain parenchymal hemorrhage, no previous ICH, and no evidence of physiological calcification on noncontrast CT of the head were included in the study. One control and two human subjects who met the inclusion criteria for the study were scanned with the same MRI protocol utilized on the phantom. The two human subjects had spontaneous basal ganglia hemorrhage and were scanned on day 7 of their hemorrhage. In the control human brain, MRI regions of interest (ROIs) were drawn in the basal ganglia region on both hemispheres. Calculations were performed on R2* maps generated from the MRI sequences (Fig. 2a). In the two human subjects, regions of interest were

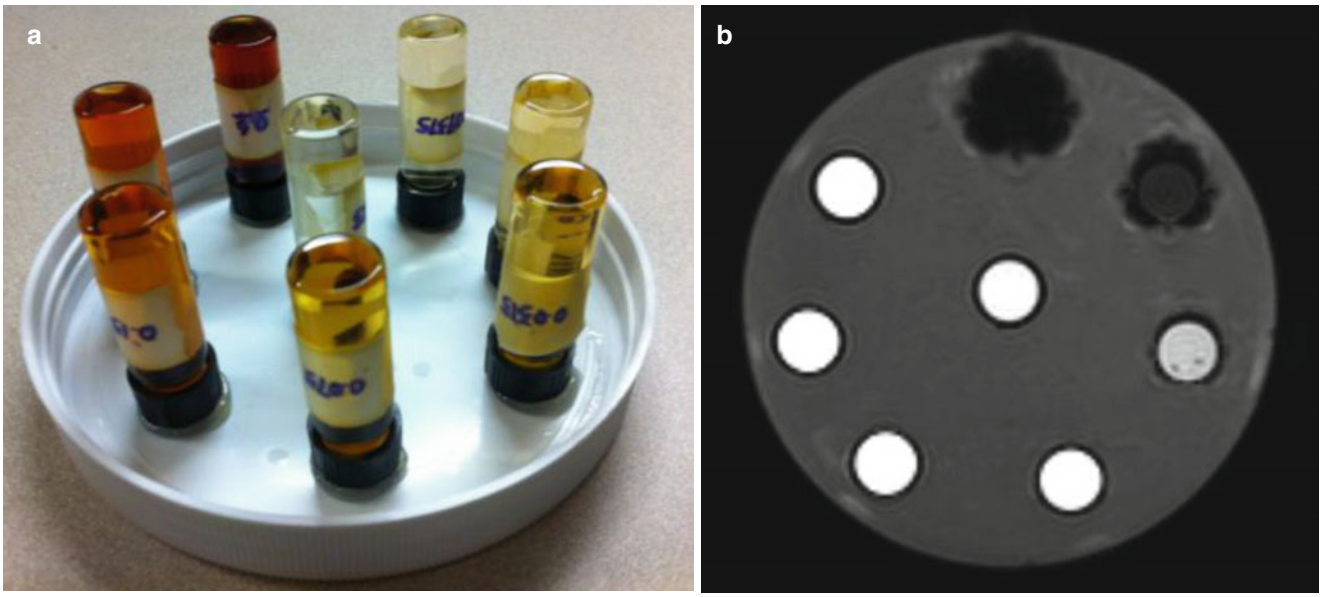


**Fig. 1** (**a**) Image of the lid of the phantom with seven 4-cc vials containing serial dilutions of iron concentration in sterile water stuck to the undersurface. (**b**) MRI of the phantom on a 3 T scanner with following sequence specifications: 3D TR = 40 ms, TE = 6.5, 11, 15.5, 20, 24.5, 29, 33.5, 38 ms, 1.5 mm slice-to-slice, acquired as 3 mm, acquired resolution matrix = 240 × 240, FOV – 240 mm × 240 mm

**Table 1** Seven serial dilutions scanned in the MRI phantom with T2* signal measurements corresponding to each concentration

| Iron concentration in the vial (mg/ml) | Corresponding MR signal magnitude ± SD |
|---|---|
| 0.6 | NA |
| 0.3 | 2.33 ± 0.46 |
| 0.15 | 3.83 ± 0.14 |
| 0.075 | 7.99 ± 0.12 |
| 0.0375 | 15.15 ± 0.29 |
| 0.01875 | 29.65 ± 0.91 |
| 0.009375 | 54.77 ± 3.85 |
| 0.0046875 | 98.23 ± 3.27 |

drawn on the periphery of the hematoma in the left basal ganglia (Fig. 2b, c). Region of interest measurements were also performed on the contralateral normal hemisphere in an identical anatomical location.

## Results

### *Control Human Subject*

In the right basal ganglia, the T2* average of three ROIs measured 44.3. In the left basal ganglia in the same control human subject, the average of three ROIs measured 53.2. Both of these measurements correspond to an iron concentration of 0.01 mg/ml.

### *First Human Subject with ICH*

Perihematomal measurements performed with three ROIs in the left basal ganglia showed T2* values of 15.3. This corresponds to an iron concentration of 0.04 mg/ml. An average of three ROIs in the contralateral normal brain in an identical anatomical location measured 49.5. This corresponds to 0.01 mg/ml of iron concentration.

### *Second Human Subject with ICH*

Perihematomal measurements performed with three ROIs in the left basal ganglia showed T2* values of 18.97. This corresponds to an iron concentration of 0.04 mg/ml. An average of three ROIs in the contralateral normal brain in an identical anatomical location measured 53.3. This corresponds to 0.01 mg/ml of iron concentration.

The above measurements demonstrate consistently that the detection of an iron concentration in the periphery of the hematoma of an ICH in the left basal ganglia on day 7 following the ictus are 4 times higher than the normal baseline concentration.

## Conclusion

Our experiment demonstrates proof of principle of MRI being able to detect a 4 times increase in tissue iron levels in the periphery of the hematoma in comparison to baseline.

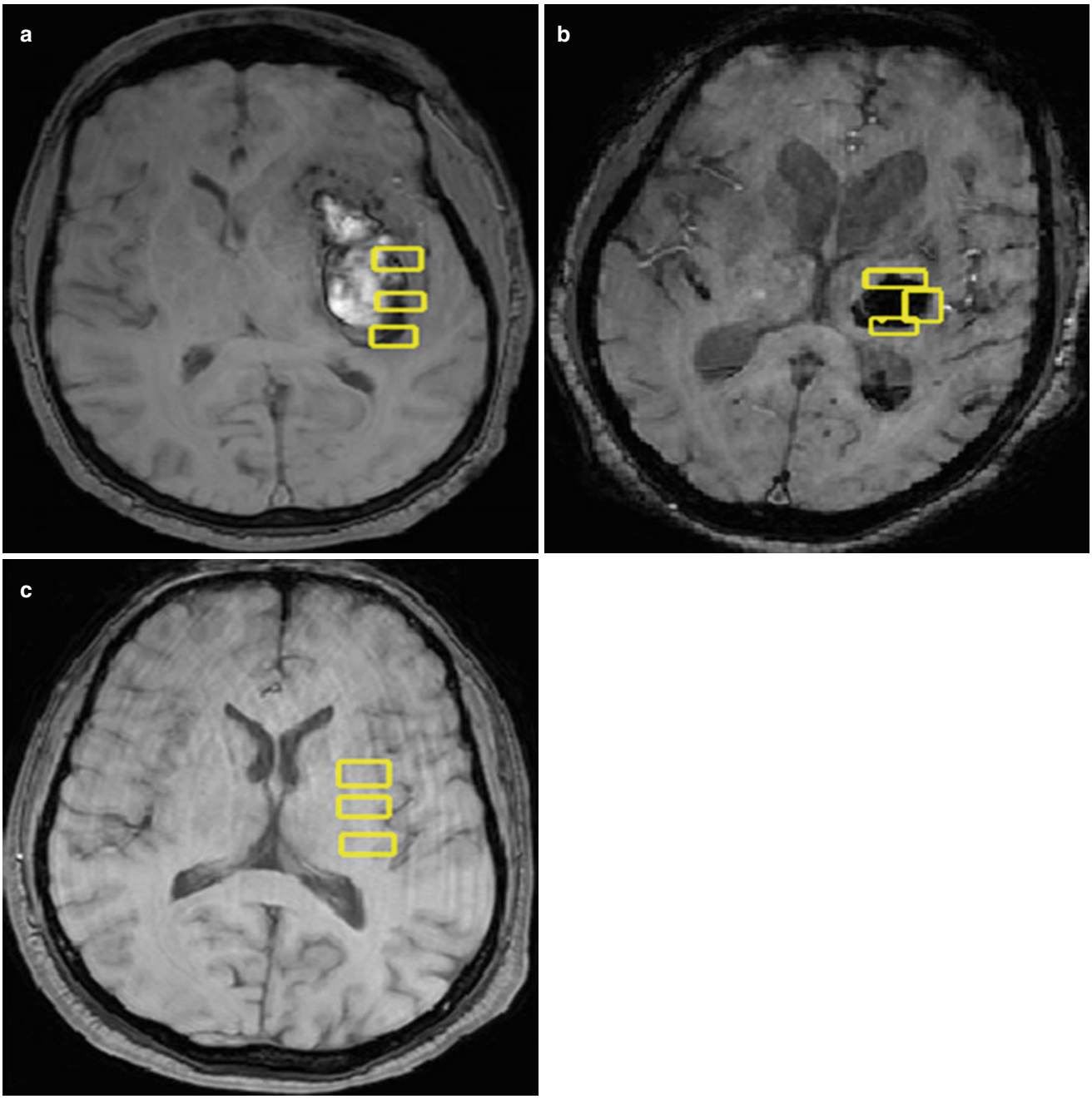


**Fig. 2** (**a**) A 70-year-old male patient with axial MRI brain showing left basal ganglia hemorrhage with regions of interest drawn for measurement of the R2* magnitude. (**b**) A 68-year-old male patient with axial MRI brain showing left basal ganglia hemorrhage with regions of interest drawn for measurement of the R2* magnitude. (**c**) A 45-year-old male subject utilized as control showing axial MRI with regions of interest drawn for baseline R2* magnitude measurement

The initial translation from bench to bedside of iron-chelating therapy with deferoxamine being investigated by a phase II trial holds promise. Our hypothesis, once validated in a larger study, can provide a surrogate marker of severity of neurotoxicity following an ICH. Moreover, an MRI-based brain tissue iron quantification may provide a more objective way of monitoring therapy with iron chelates. Furthermore, the correlation of tissue iron quantification with functional outcome following an ICH needs to be studied in a large-scale prospective analysis involving human subjects.

## References

1. Xi G, Keep RF, Hoff JT (2006) Mechanisms of brain injury after intracerebral haemorrhage. Lancet Neurol 5(1):53–63, PubMed Epub 2005/12/20
2. Morgenstern LB, Hemphill JC 3rd, Anderson C, Becker K, Broderick JP, Connolly ES Jr et al (2010) Guidelines for the management of spontaneous intracerebral hemorrhage: a guideline for healthcare professionals from the American Heart Association/American Stroke Association. Stroke 41(9):2108–2129, PubMed

3. Perez de la Ossa N, Sobrino T, Silva Y, Blanco M, Millan M, Gomis M et al (2010) Iron-related brain damage in patients with intracerebral hemorrhage. Stroke 41(4):810–813, PubMed
4. Selim M (2009) Deferoxamine mesylate: a new hope for intracerebral hemorrhage: from bench to clinical trials. Stroke 40(3 Suppl):S90–S91, PubMed
5. Wu J, Hua Y, Keep RF, Nakamura T, Hoff JT, Xi G (2003) Iron and iron-handling proteins in the brain after intracerebral hemorrhage. Stroke 34(12):2964–2969, PubMed
6. Nakamura T, Keep RF, Hua Y, Schallert T, Hoff JT, Xi G (2004) Deferoxamine-induced attenuation of brain edema and neurological deficits in a rat model of intracerebral hemorrhage. J Neurosurg 100(4):672–678, PubMed PMID: 15070122
7. Wan S, Hua Y, Keep RF, Hoff JT, Xi G (2006) Deferoxamine reduces CSF free iron levels following intracerebral hemorrhage. Acta Neurochir Suppl 96:199–202, PubMed PMID: 16671454
8. Hua Y, Nakamura T, Keep RF, Wu J, Schallert T, Hoff JT et al (2006) Long-term effects of experimental intracerebral hemorrhage: the role of iron. J Neurosurg 104(2):305–312, PubMed PMID: 16509506
9. Qureshi AI, Mendelow AD, Hanley DF (2009) Intracerebral haemorrhage. Lancet 373(9675):1632–1644, PubMed
10. Wagner KR, Sharp FR, Ardizzone TD, Lu A, Clark JF (2003) Heme and iron metabolism: role in cerebral hemorrhage. J Cereb Blood Flow Metab 23(6):629–652, PubMed
11. Pandey AS, Xi G (2014) Intracerebral hemorrhage: a multimodality approach to improving outcome. Transl Stroke Res 5(3):313–315. doi:10.1007/s12975-014-0344-z, Epub 2014 Apr 26
12. Lee KR, Colon GP, Betz AL, Keep RF, Kim S, Hoff JT (1996) Edema from intracerebral hemorrhage: the role of thrombin. J Neurosurg 84(1):91–96, PubMed
13. Xi G, Wagner KR, Keep RF, Hua Y, de Courten-Myers GM, Broderick JP et al (1998) Role of blood clot formation on early edema development after experimental intracerebral hemorrhage. Stroke 29(12):2580–2586, PubMed
14. Lee KR, Kawai N, Kim S, Sagher O, Hoff JT (1997) Mechanisms of edema formation after intracerebral hemorrhage: effects of thrombin on cerebral blood flow, blood-brain barrier permeability, and cell survival in a rat model. J Neurosurg 86(2):272–278, PubMed
15. Gebel JM, Sila CA, Sloan MA, Granger CB, Mahaffey KW, Weisenberger J et al (1998) Thrombolysis-related intracranial hemorrhage: a radiographic analysis of 244 cases from the GUSTO-1 trial with clinical correlation. Global Utilization of Streptokinase and Tissue Plasminogen Activator for Occluded Coronary Arteries. Stroke 29(3):563–569, PubMed
16. Wagner KR, Xi G, Hua Y, Kleinholz M, de Courten-Myers GM, Myers RE et al (1996) Lobar intracerebral hemorrhage model in pigs: rapid edema development in perihematomal white matter. Stroke 27(3):490–497, PubMed
17. Xi G, Keep RF, Hoff JT (1998) Erythrocytes and delayed brain edema formation following intracerebral hemorrhage in rats. J Neurosurg 89(6):991–996, PubMed
18. Huang FP, Xi G, Keep RF, Hua Y, Nemoianu A, Hoff JT (2002) Brain edema after experimental intracerebral hemorrhage: role of hemoglobin degradation products. J Neurosurg 96(2):287–293, PubMed
19. Xi G, Keep RF, Hoff JT (2002) Pathophysiology of brain edema formation. Neurosurg Clin N Am 13(3):371–383, PubMed
20. Ropper AH (1986) Lateral displacement of the brain and level of consciousness in patients with an acute hemispheral mass. N Engl J Med 314(15):953–958, PubMed
21. Enzmann DR, Britt RH, Lyons BE, Buxton JL, Wilson DA (1981) Natural history of experimental intracerebral hemorrhage: sonography, computed tomography and neuropathology. AJNR Am J Neuroradiol 2(6):517–526, PubMed
22. Tomita H, Ito U, Ohno K, Hirakawa K (1994) Chronological changes in brain edema induced by experimental intracerebral hematoma in cats. Acta Neurochir Suppl (Wien) 60:558–560, PubMed PMID: 7976649
23. Yang GY, Betz AL, Chenevert TL, Brunberg JA, Hoff JT (1994) Experimental intracerebral hemorrhage: relationship between brain edema, blood flow, and blood-brain barrier permeability in rats. J Neurosurg 81(1):93–102, PubMed PMID: 82075
24. Zazulia AR, Diringer MN, Derdeyn CP, Powers WJ (1999) Progression of mass effect after intracerebral hemorrhage. Stroke 30(6):1167–1173, PubMed
25. Ropper AH, King RB (1984) Intracranial pressure monitoring in comatose patients with cerebral hemorrhage. Arch Neurol 41(7):725–728, PubMed
26. Okauchi M, Hua Y, Keep RF, Morgenstern LB, Xi G (2009) Effects of deferoxamine on intracerebral hemorrhage-induced brain injury in aged rats. Stroke 40(5):1858–1863, PubMed Pubmed Central PMCID: 2674519
27. Okauchi M, Hua Y, Keep RF, Morgenstern LB, Schallert T, Xi G (2010) Deferoxamine treatment for intracerebral hemorrhage in aged rats: therapeutic time window and optimal duration. Stroke 41(2):375–382, PubMed PMID: 20044521
28. Gu Y, Hua Y, Keep RF, Morgenstern LB, Xi G (2009) Deferoxamine reduces intracerebral hematoma-induced iron accumulation and neuronal death in piglets. Stroke 40(6):2241–2243, PubMed Pubmed Central PMCID: 2693321
29. Selim M, Yeatts S, Goldstein JN, Gomes J, Greenberg S, Morgenstern LB et al (2011) Safety and tolerability of deferoxamine mesylate in patients with acute intracerebral hemorrhage. Stroke 42(11):3067–3074, PubMed Pubmed Central PMCID: 3202043
30. Brittenham GM, Badman DG (2003) Noninvasive measurement of iron: report of an NIDDK workshop. Blood 101(1):15–19, PubMed
31. He T, Gatehouse PD, Anderson LJ, Tanner M, Keegan J, Pennell DJ et al (2006) Development of a novel optimized breathhold technique for myocardial T2 measurement in thalassemia. J Magn Reson Imaging 24(3):580–585, PubMed
32. Raz E, Jensen JH, Ge Y, Babb JS, Miles L, Reaume J et al (2011) Brain iron quantification in mild traumatic brain injury: a magnetic field correlation study. AJNR Am J Neuroradiol 32(10):1851–1856, PubMed
33. Jensen JH, Chandra R, Ramani A, Lu H, Johnson G, Lee SP et al (2006) Magnetic field correlation imaging. Magn Reson Med 55(6):1350–1361, PubMed PMID:16700026
34. Jensen PD (2004) Evaluation of iron overload. Br J Haematol 124(6):697–711, PubMed
35. St Pierre TG, Clark PR, Chua-Anusorn W (2004) Single spin-echo proton transverse relaxometry of iron-loaded liver. NMR Biomed 17(7):446–458, PubMed
36. Jensen JH, Chandra R (2002) Theory of nonexponential NMR signal decay in liver with iron overload or superparamagnetic iron oxide particles. Magn Reson Med 47(6):1131–1138, PubMed PMID: 12111959
37. Bilgic B, Pfefferbaum A, Rohlfing T, Sullivan EV, Adalsteinsson E (2012) MRI estimates of brain iron concentration in normal aging using quantitative susceptibility mapping. Neuroimage 59(3):2625–2635, PubMed Pubmed Central PMCID: 3254708
38. Liu HL, Chen PY, Yang HW, Wu JS, Tseng IC, Ma YJ et al (2011) In vivo MR quantification of superparamagnetic iron oxide nanoparticle leakage during low-frequency-ultrasound-induced blood-brain barrier opening in swine. J Magn Reson Imaging 34(6):1313–1324, PubMed
39. Sammet CL, Swaminathan SV, Tang H, Sheth S, Jensen JH, Nunez A et al (2013) Measurement and correction of stimulated echo contamination in T2-based iron quantification. Magn Reson Imaging 31(5):664–668, PubMed
40. Wu G, Xi G, Hua Y, Sagher O (2010) T2* magnetic resonance imaging sequences reflect brain tissue iron deposition following intracerebral hemorrhage. Transl Stroke Res 1(1):31–34, PubMed
41. Wang S, Lou M, Liu T, Cui D, Chen X, Wang Y (2013) Hematoma volume measurement in gradient echo MRI using quantitative susceptibility mapping. Stroke 44(8):2315–2317. doi:10.1161/STROKEAHA.113.001638